An accurate and efficient spectral tau method for the incompressible Navier-Stokes equations in a planar channel

E.A. Coutsias* J.S. Hesthaven† J.P. Lynov‡

Abstract

We present a spectral tau method for the efficient solution of the incompressible Navier-Stokes equations in a planar channel geometry, with the Navier-Stokes equations expressed in the vorticity-stream function formulation. The main innovations of the scheme are the incorporation of no-slip constraints in the semi-implicit time advancement of the vorticity field, and the efficient and accurate solution of the linear systems, resulting from the numerical discretization of the equations, by well-conditioned integration operators. The pressure field is calculated in a post-processing step by direct inversion of the gradient. The asymptotic stability of our scheme is analyzed, and a numerical solution of the Orr-Sommerfeld stability problem for plane Poiseuille flow is performed to offer a comparison of our method of enforcing the no-slip boundary condition with that of existing techniques. Results from representative direct simulations are presented to demonstrate the accuracy of the scheme.

Key words: Tau Method, Incompressible Navier-Stokes Equations, No-slip Vorticity Constraints, Invertible Integral Operators, Pressure Calculation.

AMS subject classifications: 65M70, 76D05, 76D15, 76M25.

*Dept. of Mathematics and Statistics, University of New Mexico, Albuquerque, NM 87131. E-mail: *vageli@math.unm.edu*

†Association EURATOM – Risø National Laboratory, Optics and Fluid Dynamics Department, P.O. Box 49, DK-4000 Roskilde, Denmark. E-mail: *jsh@risoe.dk*

‡Association EURATOM – Risø National Laboratory, Optics and Fluid Dynamics Department, P.O. Box 49, DK-4000 Roskilde, Denmark. E-mail: *lynov@risoe.dk*

1 Introduction

The dynamical generation of vorticity through boundary layer interactions near material walls is a fundamental problem in both scientific and applied fluid dynamics. Although many of the problems of practical interest at high Reynolds numbers require a full three-dimensional description, there are important cases with moderately high Reynolds number in the range 100-10,000 in which a two dimensional assumption is justified. Experiments on complex boundary layer dynamics in which two-dimensionality of the flow has been emphasized have been conducted in stratified fluids [1, 2], rotating fluids [3] and in flows in which special care was taken in initially generating a two-dimensional disturbance [4, 5].

In this paper, we describe a spectral tau method for the solution of the incompressible Navier-Stokes equations in bounded geometries. Special attention is given to avoiding the serious accuracy degradation recently demonstrated [6] in high resolution polynomial approximations of high order spatial derivatives. The simplest geometry including rigid boundaries is the periodic channel, which will be used throughout. We note, however, that the method is not restricted to this geometry. We have implemented similar algorithms for the solution of flows in an annular geometry [3, 7], and coordinate transformations based on rational functions may also be applied [8].

This paper is organized as follows: In Sec. 2, the basic dynamical equations are introduced. We chose to solve the incompressible Navier-Stokes equations in the vorticity-stream function (ω–ψ) formulation. Compared to the primitive variable approach, the ω–ψ formulation reduces the number of momentum equations from two to one, it eliminates the pressure from the calculations and the incompressibility condition, $\nabla \cdot \mathbf{u} = 0$, is satisfied by construction. Section 2.1 contains equations for the viscous evolution of the total energy and enstrophy in the flow. These equations are used as accuracy checks of the code.

The vorticity-stream function formulation of flows with no-slip boundary conditions leads to an overdetermined Poisson equation relating vorticity to the stream function.

In Sec. 3, the solution of this problem via the integral solvability constraint method by Coutsias and Lynov [9] is briefly discussed, and the accuracy of this method is investigated by solution of the Orr-Sommerfeld eigenvalue problem.

Section 4 describes the implementation of the spectral scheme for the dynamical equations. Special attention is given to the use of the invertible integration operator method [8] in the accurate and efficient solution of the Poisson and Helmholtz equations. A fully discrete stability analysis of the scheme concludes this section.

The pressure does not enter the Navier-Stokes equations in the vorticity-stream function formulation, but an accurate determination of the pressure field is significant for the interpretation of the results. We have developed a method for determining the pressure field in a post-processing step based on the instantaneous vorticity field. This method, described in Sec. 5, avoids the traditional difficulties of overdeterminancy of the pressure Poisson problem and preserves the high accuracy obtained in the calculation of the vorticity.

Section 6 contains two numerical tests of the code. The first test is an unstable Poiseuille flow with the same parameters as in the Orr-Sommerfeld eigenvalue analysis, and the second test is a vortex sheet roll-up between moving no-slip walls at high Reynolds number used for investigation of the overall error of the scheme. Finally, Section 7 includes some concluding remarks.

2 Basic equations

For two-dimensional, incompressible flows it is convenient to express the Navier-Stokes equations in the vorticity-stream function formulation;

$$
\begin{aligned}
\frac{\partial \omega}{\partial t} + [\omega,\, \psi] &= \nu \nabla^2 \omega \\
\nabla^2 \psi &= -\omega \ ,
\end{aligned}
\tag{1}
$$

where the scalar vorticity field, ω, is given as

$$\nabla \times \mathbf{u} = \omega \hat{\mathbf{z}} \ ,$$

and the stream function , ψ, is related to the velocity field by

$$\mathbf{u} = (u,\, v) = \nabla \psi \times \hat{\mathbf{z}} = \left(\frac{\partial \psi}{\partial y},\, -\frac{\partial \psi}{\partial x} \right) \quad .$$

The Jacobian, $[\omega,\, \psi]$, is defined as

$$[\omega,\, \psi] = \frac{\partial \omega}{\partial x}\frac{\partial \psi}{\partial y} - \frac{\partial \psi}{\partial x}\frac{\partial \omega}{\partial y} \quad .$$

We note that the incompressibility condition is a priori satisfied in the vorticity-stream function formulation.

The normalized dynamical equations are solved in a periodic channel, $\mathcal{D}$, with no-slip walls located at $y = \pm 1$ and a periodic x-dependence of length L_x. At the impermeable walls we assume no-slip boundary conditions

$$\mathbf{u}(x, y = \pm 1, t) = U^{\pm}(t)\hat{\mathbf{x}} \ ,$$

where $U^{\pm}(t)$ signifies the time dependent horizontal velocity of the walls. In the vorticity-stream function formulation, these conditions become

$$u(x, y = \pm 1, t) = \left. \frac{\partial \psi}{\partial y} \right|_{y=\pm 1} = U^{\pm}(t) \ , \tag{2}$$

ensuring that the fluid follows the moving wall, and

$$\psi(x, y = \pm 1, t) = F^{\pm}(t) \ , \tag{3}$$

where $F^{\pm}(t)$ are arbitrary functions of time.

As may be observed from these boundary conditions, we end up with a problem of an overdetermined Poisson equation in Eq.(1) unless proper constraints are imposed on the vorticity. In Sec. 3 we will return to this problem and devise a method for deriving the appropriate no-slip solvability constraints for the vorticity.

2.1 Energy and enstrophy evolution

In the absence of viscosity, the Navier-Stokes equations, or rather the Euler equations, possess an infinite number of conserved quantities

$$E = \frac{1}{2}\int_{\mathcal{D}} |\mathbf{u}|^2 \, dS \ , \quad C_G[\omega] = \int_{\mathcal{D}} G(\omega)\, dS \ ,$$

where $\mathcal{D}$ is a planar domain, simply or multiply connected, with the velocity tangential at the boundaries. Here E is the energy, and $C_G[\omega]$ are Casimir functionals with $G(\omega)$ being an arbitrary measure of the vorticity. For the special case $G(\omega) = \omega^2$ we write

$$\Omega = \int_{\mathcal{D}} \omega^2 \, dS,$$

with Ω being the enstrophy.

For finite viscosity the temporal evolution of the energy may be derived for the present problem, yielding

$$\frac{dE}{dt} = -\nu\Omega + \nu L_x(U^-(t)\omega^- - U^+(t)\omega^+) - \delta p \int_{\mathcal{D}} \psi \, dS \ , \tag{4}$$

where $\omega^{\pm}$ is the vorticity along the moving walls at $y = \pm 1$, respectively, and δp signifies the pressure drop along one periodicity length of the channel. Using Eq.(1), we find the temporal evolution of the enstrophy

$$\frac{d\Omega}{dt} = \nu \int_{\partial\mathcal{D}} (\nabla\omega^2) \cdot \hat{\mathbf{n}} \, ds - 2\nu \int_{\mathcal{D}} (\nabla\omega)^2 \, dS \ , \tag{5}$$

where $\hat{\mathbf{n}}$ is an outward pointing normal to the boundary, $\partial\mathcal{D}$. We note that all terms originating from the interior of the flow are always negative. Thus, the only way the total energy and enstrophy may increase is by production at the boundary. These expressions are used as accuracy tests for the numerical approximations. In these tests, we compare the time derivatives obtained directly from the code, based on time centered differences of E and Ω over three consecutive time steps, with the instantaneous values determined by evaluation of the right hand sides of (4) and (5) at the center time step.

3 Vorticity boundary conditions

As discussed in Sec. 2, enforcing no-slip boundary conditions on the Navier-Stokes equations in the ω-ψ formulation leads to an overdetermined Poisson equation in Eq.(1). This problem has been addressed by several authors (see, e.g., [10, 11, 12]). Here, we will apply the method by Coutsias and Lynov [9].

The two unknown fields are expanded in Fourier series

$$\begin{pmatrix} \omega(x,y) \\ \psi(x,y) \end{pmatrix} = \sum_{j=-\infty}^{\infty} \begin{pmatrix} \hat{\omega}_j(y) \\ \hat{\psi}_j(y) \end{pmatrix} \exp\left[i \frac{2\pi}{L_x} j \, x \right] \ ,$$

where subscript j indicates the Fourier mode-number.

In this framework, the Neumann boundary conditions, Eq.(2), become

$$\left. \frac{\partial \hat{\psi}_j(y)}{\partial y} \right|_{y=\pm 1} = \begin{cases} U^{\pm}(t) & j = 0 \\ 0 & j \neq 0 \end{cases} \ . \tag{6}$$

For the Dirichlet boundary conditions, Eq.(3), we obtain

$$\hat{\psi}_j(\pm 1) = \begin{cases} F^{\pm}(t) & j = 0 \\ 0 & j \neq 0 \end{cases} \ . \tag{7}$$

In the following, we will split the treatment into two cases for $j \neq 0$ and $j = 0$.

Introducing the Fourier expansion into the Poisson equation (1) for $\underline{j \neq 0}$ yields

$$\frac{d^2 \hat{\psi}_j}{dy^2} - \lambda_j^2 \hat{\psi}_j = -\hat{\omega}_j \ , \tag{8}$$

where we have defined the coefficient

$$\lambda_j = \frac{2\pi j}{L_x} \ .$$

In Eq.(8) we have changed the y-derivative to an ordinary derivative, since time does not enter explicitly in the present discussion.

Introducing the Dirichlet Green's function, $G_j(y|s)$, we may formally write the solution, $\hat{\psi}_j(y)$, to Eq.(8) subject to the Dirichlet boundary conditions, Eq.(7), as

$$\hat{\psi}_j(y) = \int_{-1}^{1} \hat{\omega}_j(s) G_j(y|s) \, ds \ . \tag{9}$$

The Neumann condition, Eq.(6), now requires

$$\left. \frac{d\hat{\psi}_j}{dy} \right|_{\pm 1} = \int_{-1}^{1} \hat{\omega}_j(s) \left. \frac{dG_j(y|s)}{dy} \right|_{\pm 1} ds = 0 \ . \tag{10}$$

This provides necessary as well as sufficient conditions for solvability of Eq.(8) under the constraints posed by Eqs.(6)-(7) for $j \neq 0$ (note that uniqueness follows from the uniqueness of the Dirichlet problem).

Determination of the Dirichlet Green's function, $G_j(y|s)$, may be accomplished by numerical approximations. Although not a complicated task, the results can easily be contaminated by significant numerical errors, not to mention the derivative of the approximation. These problems are further discussed in [9] and [13]. Here, we simply note that it is possible do derive solvability constraints efficiently and with spectral accuracy. Expanding the Fourier coefficients, $\hat{\omega}_j$ and $\hat{\psi}_j$, in Chebyshev series

$$\begin{pmatrix} \hat{\omega}_j \\ \hat{\psi}_j \end{pmatrix} = \sum_{i=0}^{\infty} \begin{pmatrix} \hat{\omega}_{ij} \\ \hat{\psi}_{ij} \end{pmatrix} T_i(y) \ , \tag{11}$$

where $T_i(y) = \cos(i \cos^{-1} y)$ is the i-th order Chebyshev polynomial of the first kind, the solvability constraints on the vorticity expansion coefficients take the form

$$\forall j \neq 0 \ : \ \sum_{i=0}^{\infty} B_{ij}^{\pm} \hat{\omega}_{ij} = 0 \ . \tag{12}$$

The coefficients $B_{ij}^{\pm}$ are independent of time and viscosity, so they may be precalculated prior to a numerical simulation. In fact, the coefficients only depend on the geometry of the problem, i.e. L_x, besides the actual truncation of the expansions. Thus, one may, once and for all, calculate $B^{\pm}_{ij}$ with a very high truncation. These coefficients may then be applied to all problems with lower resolution for a given L_x.

For the Fourier mode $j = 0$, we note that the vorticity must maintain a circulation, C, consistent with the velocity of the walls, where

$$\begin{aligned} C &\equiv \oint_{\partial\mathcal{D}} \mathbf{u}\cdot d\mathbf{l} = L_x(U^-(t) - U^+(t)) \\ &= \int_{\mathcal{D}} \omega \, dS = L_x \int_{-1}^{1} \hat{\omega}_0(y,t)\, dy\,. \end{aligned} \tag{13}$$

Given $\hat{\omega}_0(y,t)$, Galilean invariance of the Navier-Stokes equations allows both $U^+(t)$ and $U^-(t)$ to be shifted by properly choosing a frame of reference. In the following, the choice $U^-(t) = -U^+(t)$ is made.

By integrating the x-component of the moment equation in primitive variables along the walls at $y = \pm 1$ one obtains the constraints

$$\left.\frac{\partial \hat{\omega}_0}{\partial y}\right|_{y=\pm 1} = -\frac{1}{\nu L_x}\delta p - \frac{1}{\nu}\frac{d}{dt}U^{\pm}(t)\,, \tag{14}$$

where δp is the total pressure difference along a length of period of the channel. The two conditions in (14) are consistent with the circulation requirement (13), so any two of the three conditions can be used as constraints. We will return to this issue in Sec. 4.2.2.

When solving the Poisson equation for ψ during the simulation, Dirichlet boundary conditions are used for $j \neq 0$ and Neumann conditions for $j = 0$. This leaves us the freedom to choose

$$\hat{\psi}_{00} = 0\,.$$

3.1 Solution of the Orr-Sommerfeld equation

In order to study the accuracy of the solvability constraints and ensure the consistency of the scheme, we now address the Orr-Sommerfeld equation in the vorticity-stream function formulation. Assuming we may express

$$\psi(x,y,t) = \psi(y) + \tilde{\psi}(x,y,t)$$

and

$$\omega(x,y,t) = \omega(y) + \tilde{\omega}(x,y,t) \quad ,$$

we obtain, by linearizing Eq.(1) around the solution

$$u_0 = \frac{\partial \psi}{\partial y} = U(y) \;\text{ and }\; v_0 = -\frac{\partial \psi}{\partial x} = 0 \quad ,$$

the equations

$$\frac{\partial \tilde{\omega}}{\partial t} + U''\frac{\partial \tilde{\psi}}{\partial x} + U\frac{\partial \tilde{\omega}}{\partial x} = \nu \nabla^2 \tilde{\omega} \quad , \tag{15}$$

$$\nabla^2 \tilde{\psi} = -\tilde{\omega} \quad . \tag{16}$$

As boundary conditions we obtain

$$\tilde{\psi}(x,\pm 1,t) = \left.\frac{\partial \tilde{\psi}}{\partial y}\right|_{y=\pm 1} = 0 \quad , \tag{17}$$

assuming that we consider only stream-wise perturbations with non-zero wave-numbers. Following the standard procedure for temporal stability analysis we express the perturbations as

$$\begin{aligned} \tilde{\omega} &= e^{\lambda t}[\omega^c(y)\cos(\alpha k x) + \omega^s(y)\sin(\alpha k x)] \quad , \\ \tilde{\psi} &= e^{\lambda t}[\psi^c(y)\cos(\alpha k x) + \psi^s(y)\sin(\alpha k x)] \quad , \end{aligned}$$

where $k \in \mathrm{N}^+$ is the wave number along the channel, $\alpha = 2\pi/L_x$ is the aspect ratio and $\lambda = \lambda_r + i\,\lambda_i \in \mathrm{C}$ expresses the complex frequency of the initial perturbation. For $\lambda_r > 0$ we have temporal instability, and for $\lambda_r < 0$ we have temporal stability of the initial perturbation.

Introducing these expressions into Eqs.(15)-(17) gives the Orr-Sommerfeld eigenvalue problem. By this procedure the eigenvalue problem is expressed as two coupled second order differential equations. This form is different from the single fourth order equation obtained in the classical pure stream function formulation (see, e.g., [14]). Our formulation offers the opportunity to compare results obtained either by applying the four boundary conditions on the stream function, as in the usual approach, or the Dirichlet boundary conditions on the stream function and the solvability constraints on the vorticity.

In order to solve the Orr-Sommerfeld equation, we follow the pioneering work by Orszag [14]. Thus, we approximate all unknowns by truncated Chebyshev series as

$$\begin{pmatrix} \psi^c(y) \\ \psi^s(y) \\ \omega^c(y) \\ \omega^s(y) \\ U(y) \end{pmatrix} \approx \sum_{i=0}^{M} \begin{pmatrix} \hat{\psi}^c_i \\ \hat{\psi}^s_i \\ \hat{\omega}^c_i \\ \hat{\omega}^s_i \\ \hat{U}_i \end{pmatrix} T_i(y) \quad .$$

Due to the even-odd symmetry of the Orr-Sommerfeld equation it is sufficient to consider the even Chebyshev modes, only. However, for simplicity we have have chosen not to take advantage of this property.

Introducing these expansions yields the following set of equations for each Chebyshev mode (i);

$$
\begin{aligned}
&-\nu\left[\mathbf{D}_i^2\hat{\omega}^c-(\alpha k)^2\hat{\omega}_i^c\right]+\alpha k\mathbf{C}_i(\hat{U},\,\hat{\omega}^s)+\\
&\qquad\alpha k\mathbf{C}_i(\mathbf{D}^2\hat{U},\,\hat{\psi}^s)=-\lambda\hat{\omega}_i^c\\
&-\nu\left[\mathbf{D}_i^2\hat{\omega}^s-(\alpha k)^2\hat{\omega}_i^s\right]-\alpha k\mathbf{C}_i(\hat{U},\,\hat{\omega}^c)-\\
&\qquad\alpha k\mathbf{C}_i(\mathbf{D}^2\hat{U},\,\hat{\psi}^c)=-\lambda\hat{\omega}_i^s\\
&\mathbf{D}_i^2\hat{\psi}^c-(\alpha k)^2\hat{\psi}_i^c+\hat{\omega}_i^c=0\\
&\mathbf{D}_i^2\hat{\psi}^s-(\alpha k)^2\hat{\psi}_i^s+\hat{\omega}_i^s=0\ ,
\end{aligned}
\tag{18}
$$

where k is the stream-wise mode-number. For convenience, we have introduced the symbols

$$\mathbf{D}_i^2\hat{f}=\frac{1}{c_i}\sum_{\substack{p=i+2\\ p+i\ \text{even}}}^{M}p(p^2-i^2)\hat{f}_p\ ,$$

for the second order spectral differential operator, $\mathbf{D}^2$, [16], and

$$\mathbf{C}_i(\hat{f},\,\hat{g})=\frac{1}{2c_i}\sum_{m=-M}^{M}\hat{f}_{|m-i|}\hat{g}_{|m|}c_{|m-i|}c_{|m|}\ ,$$

for the convolution operator [14]. Here $\hat{f}=(\hat{f}_0,\ldots,\hat{f}_M)^T$, $\hat{g}=(\hat{g}_0,\ldots,\hat{g}_M)^T$, and $c_0=2$, $c_i=0$ for $i<0$ and $c_i=1$ for $i>0$.

In this context, the four boundary conditions (17) on the stream function become

$$\sum_{i=0}^{M}(\pm1)^i\hat{\psi}_i^c=0\ ,\ \sum_{i=0}^{M}(\pm1)^i\hat{\psi}_i^s=0\ ,\tag{19}$$

$$\sum_{i=0}^{M}(\pm1)^{i+1}i^2\hat{\psi}_i^c=0\ ,\ \sum_{i=0}^{M}(\pm1)^{i+1}i^2\hat{\psi}_i^s=0\ ,\tag{20}$$

Alternatively, we may enforce the vorticity constraints (7) and (12) as

$$\sum_{i=0}^{M}(\pm1)^i\hat{\psi}_i^c=0\ ,\ \sum_{i=0}^{M}(\pm1)^i\hat{\psi}_i^s=0\ ,\tag{21}$$

$$\sum_{i=0}^{M}B_{ik}^{\pm}\hat{\omega}_i^c=0\ ,\ \sum_{i=0}^{M}B_{ik}^{\pm}\hat{\omega}_i^s=0\ .\tag{22}$$

Defining the eigenvector of the problem as

$$\mathbf{x}=(\hat{\omega}_0^c,\ldots,\hat{\omega}_M^c,\hat{\omega}_0^s,\ldots,\hat{\omega}_M^s,\hat{\psi}_0^c,\ldots,\hat{\psi}_M^c,\hat{\psi}_0^s,\ldots,\hat{\psi}_M^s)^T\ ,$$

Eq.(18) may be recast as a generalized eigenvalue problem;

$$\mathbf{A}\,\mathbf{x}=\lambda\mathbf{B}\,\mathbf{x}\ ,$$

where $\mathbf{A}$ and $\mathbf{B}$ are 4×4 general block-matrices of order $M+1$, given as

$$
\begin{aligned}
\mathbf{A}&=\begin{bmatrix}\mathbf{Q}^4&\mathbf{Q}^2&0&\mathbf{Q}^3\\-\mathbf{Q}^2&\mathbf{Q}^4&-\mathbf{Q}^3&0\\\mathbf{I}&0&\mathbf{Q}^1&0\\0&\mathbf{I}&0&\mathbf{Q}^1\end{bmatrix}\ ,\\
\mathbf{B}&=\begin{bmatrix}-\mathbf{I}&0&0&0\\0&-\mathbf{I}&0&0\\0&0&0&0\\0&0&0&0\end{bmatrix}\ .
\end{aligned}
\tag{23}
$$

Here $\mathbf{I}$ is the identity matrix and the block matrices are defined by row, i, as

$$
\begin{array}{ll}
\mathbf{Q}_i^1=\mathbf{D}_i^2-(\alpha k)^2\mathbf{I}_i & \mathbf{Q}_i^3=\alpha k\mathbf{C}_i(\mathbf{D}_i^2\hat{U},\,\cdot)\\
\mathbf{Q}_i^2=\alpha k\mathbf{C}_i(\hat{U},\,\cdot) & \mathbf{Q}_i^4=-\nu\mathbf{Q}_i^1
\end{array}\ .
$$

The boundary conditions are applied as tau-conditions, included in the two bottom rows of the submatrices.

Applying the boundary conditions on the stream function only is done by putting the Neumann conditions, Eq.(20), in the bottom rows of submatrix $\mathbf{A}_{13}$ and $\mathbf{A}_{24}$. The Dirichlet conditions, Eq.(19), are applied in the submatrices $\mathbf{A}_{33}$ and $\mathbf{A}_{44}$.

Alternatively, enforcing the vorticity constraints is performed by applying the Dirichlet boundary conditions on the stream function, Eq.(21), in the submatrices $\mathbf{A}_{33}$ and $\mathbf{A}_{44}$, and the solvability constraints on the vorticity, Eq.(22), in the submatrices $\mathbf{A}_{11}$ and $\mathbf{A}_{22}$.

The actual eigenvalue calculations are performed using the QZ-algorithm [15] on a SUN Sparc 2 in double precision and a floating point accuracy of 10^{-16}. To select actual eigenvalues from spurious ones, the calculation is done for increasing number of modes in the expansions, and only eigenvalues which vary by a small amount, $\mathcal{O}(10^{-4})$, when increasing M are considered as being adequately resolved.

For comparing the two different types of boundary conditions, we consider the standard test case of a Poiseuille flow with a velocity profile given as

$$U(y)=U_0(1-y^2)\ .\tag{24}$$

We set the channel length, $L_x=2\pi$ (i.e. $\alpha=1.0$), $k=1$, $U_0=1.0$ and $\mathrm{Re}=1/\nu=10000$. For this case, it is well known that only one linearly unstable mode exists. Orszag [14] found the frequency and the growth rate of this mode to be

$$\lambda_i=0.23752649\quad\lambda_r=0.00373967\ ,$$

to within one part in 10^8. He approached the problem in a way similar to what is done here, but kept the fourth-order operator in the stream function formulation.

M	λ_i	λ_r	ε
28	0.2375725805	0.0037438270	2E-03
32	0.2375578883	0.0037060035	4E-05
36	0.2375268225	0.0037340707	4E-05
40	0.2375259476	0.0037391415	5E-06
44	0.2375264073	0.0037396184	6E-07
48	0.2375264823	0.0037396728	9E-08
52	0.2375264879	0.0037396698	6E-09
56	0.2375264888	0.0037396708	1E-09
60	0.2375264888	0.0037396706	1E-10
64	0.2375264888	0.0037396706	3E-11
68	0.2375264888	0.0037396706	5E-10
72	0.2375264888	0.0037396706	5E-10
76	0.2375264888	0.0037396706	1E-11
80	0.2375264859	0.0037396727	4E-09
84	0.2375264882	0.0037396710	3E-09
88	0.2375264905	0.0037396694	3E-09

Table 1: Frequency, λ_i, and growth rate, λ_r, for the Orr-Sommerfeld problem at Re $= 1/\nu = 10000$, $k = 1, \alpha = 1.0$ and $U_0 = 1.0$ As boundary conditions are used the four conditions on the stream function. $\varepsilon = |\lambda_M - \lambda_{M-2}|^2$ shows the convergence of the eigenvalue corresponding to the first unstable mode for increasing M.

M	λ_i	λ_r	ε
28	0.2375702251	0.0037455732	2E-03
32	0.2375586386	0.0037057074	4E-05
36	0.2375267517	0.0037342618	4E-05
40	0.2375259549	0.0037390797	5E-06
44	0.2375264096	0.0037396332	7E-07
48	0.2375264811	0.0037396693	8E-08
52	0.2375264882	0.0037396706	7E-09
56	0.2375264888	0.0037396706	5E-10
60	0.2375264888	0.0037396706	2E-11
64	0.2375264888	0.0037396706	3E-11
68	0.2375264888	0.0037396706	7E-11
72	0.2375264888	0.0037396706	4E-11
76	0.2375264888	0.0037396706	2E-10
80	0.2375264889	0.0037396706	3E-10
84	0.2375264888	0.0037396705	1E-10
88	0.2375264887	0.0037396706	1E-10

Table 2: Frequency, λ_i, and growth rate, λ_r, for the Orr-Sommerfeld problem at Re $= 1/\nu = 10000$, $k = 1, \alpha = 1.0$ and $U_0 = 1.0$. As boundary conditions are used the Dirichlet boundary conditions for the stream function and the solvability constraint for the vorticity. $\varepsilon = |\lambda_M - \lambda_{M-2}|^2$ shows the convergence of the eigenvalue corresponding to the first unstable mode for increasing M.

In Table 1 we show the result of the eigenvalue calculation with the boundary conditions given by Eqs.(19)-(20). We observe excellent agreement with the results reported in [14], but also note that for $M > 76$ the solution is contaminated by round-off errors.

In Table 2 we show the results of stability calculations with the boundary conditions enforced through the vorticity constraints. Again we observe excellent agreement with previously published results. This clearly proves the consistency between the two types of boundary conditions. It seems that enforcing the solvability constraints leads to slightly more accurate results for large number of modes (M). This may be due to better conditioned matrices when the solvability constraints are applied as opposed to the Neumann type boundary conditions, thereby reducing the effects of round-off errors. We are able to calculate the unstable eigenvalues with an accuracy of $\mathcal{O}(10^{-10})$.

4 Implementation

Having developed consistent solvability constraints for the vorticity, we proceed now by presenting a full implementation of a spectral scheme for solving Navier-Stokes equations in a two-dimensional channel. Additionally, we will address the issues of solution of implicit problems, the determination of the initial vorticity distribution, and the question of full discrete stability of the proposed scheme.

4.1 General description

We approximate the two unknown variables, ω and ψ, by a truncated Fourier-Chebyshev expansion, i.e.

$$\begin{aligned} &\begin{pmatrix} \omega(x,y,t) \\ \psi(x,y,t) \end{pmatrix} \approx \\ &\sum_{i=0}^{M} \sum_{j=0}^{N/2} \left[\begin{pmatrix} \hat{\omega}^c_{ij} \\ \hat{\psi}^c_{ij} \end{pmatrix} \cos\left(\frac{2\pi j}{L_x} x\right) + \begin{pmatrix} \hat{\omega}^s_{ij} \\ \hat{\psi}^s_{ij} \end{pmatrix} \sin\left(\frac{2\pi j}{L_x} x\right) \right] T_i(y) \ , \end{aligned} \tag{25}$$

where $\hat{\omega}^c_{ij}$, $\hat{\omega}^s_{ij}$, $\hat{\psi}^c_{ij}$ and $\hat{\psi}^s_{ij}$ are the expansion coefficients.

In the remaining part we will use, $\hat{\omega}_{ij}$ and $\hat{\psi}_{ij}$ as symbols for both cosine and sine-modes, as their treatment will be equivalent. Also, we will use $\hat{\omega}$ and $\hat{\psi}$ as symbols for the full matrices of unknown expansion coefficients.

This recasts Eq.(1) into

$$\begin{aligned} \frac{\partial \hat{\omega}}{\partial t} + [\hat{\omega}, \hat{\psi}] &= \nu \nabla^2 \hat{\omega} \\ \nabla^2 \hat{\psi} &= -\hat{\omega} \ , \end{aligned}$$

with boundary conditions given by Eqs. (6)-(7). The Jacobian, $[\cdot,\cdot]$, becomes a two-dimensional convolution in mode space. However, in order to avoid the significant computational load required to calculate the convolution, the derivatives are calculated in mode space, whereas the convolution is done in point-space, where it amounts to a pointwise multiplication. Immediately after transforming the Jacobian back to mode-space, it is fully de-aliased using the 2/3-rule.

For time integration of the spectral equation, the presence of a nonlinear convective term and a linear diffusive term offers itself to semi-implicit time integration. We have chosen to apply a fully corrected 3rd order predictor-corrector Adams-Bashforth scheme for the convective term and a backward Euler for the diffusive term. This leads to a full scheme for advancing one time step, (n), as

$$\begin{aligned}
&\nabla^2\hat{\psi}^n = -\hat{\omega}^n \\
\text{(P):}\ &\left(1-\nu\Delta t\nabla^2\right)\hat{\omega}^* = \\
&\qquad \hat{\omega}^n + \frac{\Delta t}{12}\left(23F^n - 16F^{n-1} + 5F^{n-2}\right) \\
&\nabla^2\hat{\psi}^* = -\hat{\omega}^* \\
\text{(C):}\ &\left(1-\nu\Delta t\nabla^2\right)\hat{\omega}^{n+1} = \\
&\qquad \hat{\omega}^n + \frac{\Delta t}{12}\left(5F^* + 8F^n - F^{n-1}\right) \quad ,
\end{aligned} \tag{26}$$

where P and C denote the predictor and the corrector step, respectively, Δt is the time step and

$$F^n = -[\hat{\omega}^n,\ \hat{\psi}^n] \quad .$$

In the next two sections we will address the problems of how to solve the two implicit equations and discuss the stability of the full discrete scheme.

4.2 Solution of the implicit problems

As seen in the previous section, our scheme requires a Poisson and Helmholtz equation to be solved twice in every time step. This puts significant requirements on the efficiency and accuracy of the methods applied to solve these implicit equations.

For the present scheme we have applied some recent results by Coutsias et al. [8] by which both problems may be reduced to operations on well-conditioned tri-diagonal matrices. In order to understand the idea behind the schemes, we leave for a moment the full two-dimensional problems and consider the simple one-dimensional Poisson equation

$$\frac{\partial^2 u}{\partial x^2} = f \quad , \quad u(\pm 1) = 0 \quad , \tag{27}$$

where $u = u(x),\ f = f(x)$ and $x \in [-1, 1]$.

In constructing an approximate solution to this problem, using a Chebyshev tau method, we look for solutions to

$$\mathbf{L}_M \hat{u} = \hat{f} \quad ,$$

where

$$\begin{pmatrix} u(x) \\ f(x) \end{pmatrix} \approx \sum_{i=0}^{M} \begin{pmatrix} \hat{u}_i \\ \hat{f}_i \end{pmatrix} T_i(x) \quad ,$$

such that $\hat{u} = (\hat{u}_0, \ldots, \hat{u}_M)^T \in Q_0^M \equiv span\{T_i\}_{i=0}^M$ and $\hat{f} = (\hat{f}_0, \ldots, \hat{f}_M)^T \in Q_0^{M-2}$. In this case $\mathbf{L}_M = \mathbf{D}^2$, which is the second order differentiation matrix as given in e.g. [16]. This operator has, in the absence of boundary conditions, a strict upper triangular form. Applying the boundary conditions as tau conditions in the lowest two rows results in a non-singular matrix problem. Solution of this problem by direct methods, e.g. Gaussian elimination, requires $\mathcal{O}(M^3)$ operations. Additionally, for increasing resolution, M, this problem becomes ill-conditioned and, thus, introduces significant numerical errors, which may inhibit dynamical studies where the Poisson equation is solved repeatedly.

For these reasons, we approach the problem differently. Following [8], we assume that $Q_0^M = \mathcal{N}(\mathbf{D}^2) \oplus Q_2^M$ where $\mathcal{N}(\mathbf{D}^2)$ signifies the null-space of the operator, $\mathbf{D}^2$. The approximate solution to Eq.(27) may be obtained as

$$\hat{u} = \hat{u}^p + \sum_{k=0}^{1} \alpha_k\, \hat{e}^k \quad , \tag{28}$$

where $\hat{u}^p \in Q_2^M$ is a particular solution, $\hat{e}^k = (\hat{e}_0^k, \ldots, \hat{e}_M^k)^T$ and $span\{\hat{e}_k\}_{k=0}^1 = \mathcal{N}(\mathbf{D}^2)$ spans the null-space of the operator, i.e. it is a basis for the homogeneous solutions. We will later return to the determination of the two constants, α_k. By identifying these different spaces, we obtain that the operator, $\tilde{\mathbf{D}}^2 : Q_2^M \to Q_0^{M-2}$, is a 1-1 mapping in the restricted domain with a uniquely defined inverse, $\tilde{\mathbf{D}}^{-2} : Q_0^{M-2} \to Q_2^M$. We may conveniently term the inverse operator an integration operator. As shown by Coutsias et al. [8], this operator can be determined from the recursion relations of the orthogonal polynomial family. For the Chebyshev basis, it has the elements for $\forall i \in [2, \ldots, M]$

$$\tilde{\mathbf{D}}_{ij}^{-2} = \begin{cases} \frac{c_{i-2}}{4i(i-1)} & j = i-2 \\ -\frac{1}{2(i^2-1)} & j = i \\ \frac{1}{4i(i+1)} & j = i+2 \\ 0 & \text{otherwise} \end{cases} \quad , \tag{29}$$

i.e. it is simply a tri-diagonal matrix, with the first two rows being zeros. Having identified the integration operator allows us to derive an algorithm for solving the Poisson equation in $\mathcal{O}(M)$ operations.

The particular solution in Eq.(28), may be found straightforwardly as

$$\hat{u}^p = \tilde{\mathbf{D}}^{-2}\hat{f} \quad . \tag{30}$$

In order to obtain the full solution, we need to identify the null-space of the operator. We assume that $\hat{e}^k = \hat{\delta}^k + \hat{q}^k$, where $\hat{e}^k \in Q_0^M$, $\hat{q}^k \in Q_2^M$ and $\hat{\delta}^k$ signifies a vector of zeroes with the k'th position being one. This is simply the Chebyshev transform of T_k. Since $\hat{e}^k$ is a null-vector to the operator, $\tilde{\mathbf{D}}^2$, we obtain

$$\forall k \in [0,1]: \ \mathbf{D}^2\hat{e}^k = \mathbf{D}^2(\hat{\delta}^k + \hat{q}^k) = 0 \quad ,$$

or

$$\tilde{\mathbf{D}}^2\hat{q}^k = 0 \quad ,$$

since $\mathbf{D}^2\hat{\delta}_k \equiv 0$. In this simple example, this equation only has the trivial solution. Thus, we obtain the null-space of the operator as

$$\hat{e}^0 = \hat{\delta}^0 \quad , \quad \hat{e}^1 = \hat{\delta}^1 \quad .$$

The complete solution may them be written, using Eq.(28), as

$$\hat{u} = \hat{u}^p + \alpha_0\hat{\delta}^0 + \alpha_1\hat{\delta}^1 \quad .$$

Introducing the boundary conditions, we obtain the two unknown constants as the solution to a 2×2 system;

$$\begin{aligned} x = -1 \quad &: \quad \sum_{i=0}^{M} \hat{u}_i^p(-1)^i \ + \ \alpha_0 \ - \ \alpha_1 = 0 \\ x = 1 \quad &: \quad \sum_{i=0}^{M} \hat{u}_i^p \ + \ \alpha_0 \ + \ \alpha_1 = 0 \quad . \end{aligned}$$

As we have seen, once the particular solution is found in $\mathcal{O}(M)$ operations using Eq.(30), the remaining part of the solution amounts to solving a 2×2 system. As shown in [8], the conditioning of the integration operator is very good, leading us to the conclusion that the full problem may be solved with very high accuracy even at high resolution.

4.2.1 Poisson's equation

Following the approach outlined in the previous part of the paper, we will now derive an algorithm, based on the integration operators, for solving the two-dimensional Poisson equation in a channel geometry.

Expanding the unknowns in a truncated Fourier(N)-Chebyshev(M) series yields the following problem for $\forall j \in [0, \ldots, N/2]$

$$\left[\mathbf{D}^2 - (j\alpha)^2\mathbf{I}\right]\hat{\psi}_j = -\hat{\omega}_j \quad , \tag{31}$$

where $\alpha = 2\pi/L_x$ is the aspect ratio, $\mathbf{I}$ is the identity matrix and $\hat{\psi}_j = (\hat{\psi}_{0j}, \ldots, \hat{\psi}_{Mj})^T$, $\hat{\omega}_j = (\hat{\omega}_{0j}, \ldots, \hat{\omega}_{Mj})^T$. Thus, all the Fourier modes decouple, and we have to solve N independent equations of the form given by Eq.(31). The boundary conditions were derived in Sec. 3 as

$$\begin{aligned} j = 0 \quad &: \quad \hat{\psi}_{00} = 0 \ , \quad \sum_{i=0}^{M}(\pm 1)^{i+1} i^2 \hat{\psi}_{i0} = U^{\pm}(t) \\ j \neq 0 \quad &: \quad \sum_{i=0}^{M}(\pm 1)^i \hat{\psi}_{ij} = 0 \quad . \end{aligned} \tag{32}$$

We now introduce $\hat{\xi}_j = \tilde{\mathbf{D}}^2\hat{\psi}_j^p$, $\hat{\xi}_j \in Q_0^{M-2}$, leading to an approach for obtaining the particular solution as

$$\begin{aligned} &\left[\mathbf{I} - (j\alpha)^2\tilde{\mathbf{D}}^{-2}\right]\hat{\xi}_j = -\hat{\omega}_j \\ &\hat{\psi}_j^p = \tilde{\mathbf{D}}^{-2}\hat{\xi}_j \quad . \end{aligned} \tag{33}$$

We note that all matrices are tri-diagonal matrices such that the problem may be solved efficiently by forward substitution. The only remaining part is to identify the null-space of the operator. Similar to what was done for the one-dimensional Poisson problem, we assume, $\hat{e}_j^k = \hat{\delta}^k + \hat{q}_j^k$, such that

$$\begin{aligned} &\left[\mathbf{D}^2 - (j\alpha)^2\mathbf{I}\right]\hat{e}_j^k = \left[\mathbf{D}^2 - (j\alpha)^2\mathbf{I}\right](\hat{\delta}^k + \hat{q}_j^k) = 0 \quad \Rightarrow \\ &\left[\tilde{\mathbf{D}}^2 - (j\alpha)^2\mathbf{I}\right]\hat{q}_j^k = (j\alpha)^2\hat{\delta}^k \quad . \end{aligned} \tag{34}$$

Assuming $\hat{\xi}_j^k = \tilde{\mathbf{D}}^2\hat{q}_j^k$ one obtains the scheme

$$\begin{aligned} &\left[\mathbf{I} - (j\alpha)^2\tilde{\mathbf{D}}^{-2}\right]\hat{\xi}_j^k = (j\alpha)^2\hat{\delta}^k \\ &\hat{q}_j^k = \tilde{\mathbf{D}}^{-2}\hat{\xi}_j^k \\ &\hat{e}_j^k = \hat{\delta}^k + \hat{q}_j^k \quad . \end{aligned} \tag{35}$$

Contrary to the simpler case of the one-dimensional Poisson equation, we cannot obtain the null-vector by analytical means. However, one should note that the null-vector may be calculated in a preprocessing stage. Since all operations only involve well-conditioned tri-diagonal banded matrices the eigenvectors spanning the null-space may be found with high accuracy.

Introduction of the boundary conditions is done by applying Eq.(28). The treatment may conveniently be split into zero and non-zero Fourier modes.

Fourier mode $j \neq 0$:

Following Eq.(32) we obtain

$$\begin{aligned}(36)\quad &\sum_{i=0}^{M} \hat{\psi}^p_{ij} + \alpha_0 \sum_{i=0}^{M} \hat{e}^0_{ij} + \alpha_1 \sum_{i=0}^{M} \hat{e}^k_{ij} = 0\\ &\sum_{i=0}^{M}(-1)^i\hat{\psi}^p_{ij} + \alpha_0 \sum_{i=0}^{M}(-1)^i\hat{e}^0_{ij} + \alpha_1 \sum_{i=0}^{M}(-1)^i\hat{e}^k_{ij} = 0 \ .\end{aligned}$$

Note that summation over the null-vectors may be done as preprocessing. Thus, calculating the two constants α_0 and α_1 is an $\mathcal{O}(M)$ operation.

Fourier mode $j = 0$:

In this case the problem becomes equivalent to the example in the beginning of this section. Thus, $\hat{q}^k_0 \equiv 0$. Since we choose $\hat{\psi}_{00} = 0$ we obtain the solution

$$\hat{\psi}_0 = \hat{\psi}^p_0 + \alpha_1 \delta^1 \ .$$

As a consequence we are only able to specify the value of $\hat{\psi}_0(y)$ at one boundary which is in full accordance with what we found in Sec. 3. As the problem is overdetermined, we will give two different ways, which, however, are fully consistent.

Using the Neumann conditions leads to

$$(37)\qquad \alpha_1 = U^{\pm}(t) - \sum_{i=0}^{M}(\pm 1)^{i+1} i^2\, \hat{\psi}_{i0} \ .$$

Alternatively, one may apply the two constraints simultaneously by adding the two expressions to obtain a condition restricting the odd coefficients

$$(38)\qquad \alpha_1 = \frac{1}{2}\left(U^+(t) - U^-(t)\right) - \sum_{\substack{i=1\\ i \text{ odd}}}^{M-1} i^2 \hat{\psi}^p_{i0} \ .$$

As it has been shown, it is possible to construct the scheme such that all operations are performed using banded matrices. This reduces the total operation count to $\mathcal{O}(MN)$ as compared to the direct method being an $\mathcal{O}(M^3N)$ operation. In addition to this, all matrices are well-conditioned and the boundary conditions do not introduce any additional round-off error into the problem as is often the case when using traditional tau methods.

In the absence of the boundary conditions, the tri-diagonal form of the Poisson equation presented here is equivalent to that proposed in [16]. However, we wish to emphasize that this particular tri-diagonal form here is shown to be a consequence of the three term recurrence relation for the Chebyshev polynomial and not of the specific geometry. Similar banded operators may be obtained for all polynomials obeying such a recurrence relation.

4.2.2 Helmholtz' equation

The scheme for the Helmholtz equation is very similar to that of the Poisson equation. Consider the Helmholtz equation approximated by a Fourier-Chebyshev series

$$(39)\qquad \left[\lambda \mathbf{D}^2 - (1 + \lambda (j\alpha)^2)\mathbf{I}\right] \hat{\omega}_j = \hat{f}_j \ ,$$

for $\forall j \in [0, \ldots, N/2]$, where $\lambda = \nu \Delta t$. As for the Poisson problem, all Fourier modes decouple. The solvability constraints for the vorticity were derived in Sec. 3 as

$$(40)\qquad \begin{aligned} j = 0 :&\\ &\sum_{i=0}^{M}(\pm 1)^{i+1} i^2 \hat{\omega}_{i0} = -\frac{1}{\nu L_x}\delta p - \frac{1}{\nu}\frac{d}{dt}U^{\pm}(t) \quad \text{or}\\ &-\frac{C}{2L_x} = U^-(t) - U^+(t) = \sum_{\substack{i=0\\ i \text{ even}}}^{M} \frac{\hat{\omega}_{i0}}{i^2 - 1}\\ j \neq 0 :&\\ &\sum_{i=0}^{M} B^{\pm}_{ij}\hat{\omega}_{ij} = 0 \ .\end{aligned}$$

As for the Poisson problem, direct solution leads to an ill-conditioned problem for large resolution. We introduce $\hat{\xi}_j = \tilde{\mathbf{D}}^2 \hat{\omega}^p_j$ leading to an approach for obtaining the particular solution as

$$(41)\qquad \begin{aligned}&\left[\lambda \mathbf{I} - (1 + \lambda (j\alpha)^2)\tilde{\mathbf{D}}^{-2}\right] \hat{\xi}_j = \hat{f}_j\\ &\hat{\omega}^p_j = \tilde{\mathbf{D}}^{-2}\hat{\xi}_j \ .\end{aligned}$$

We note in particular that all matrices are tri-diagonal matrices such that the problem may be solved efficiently by forward substitution. The only remaining part is to identify the null-space of the operator. We define the null-vector as $\hat{e}^k_j = \hat{\delta}^k + \hat{q}^k_j$, to obtain

$$(42)\qquad \left[\lambda \mathbf{D}^2 - (1 + \lambda (j\alpha)^2)\mathbf{I}\right] \hat{q}^k_j = (1 + \lambda (j\alpha)^2)\hat{\delta}^k \ .$$

Assuming $\hat{\xi}^k_j = \tilde{\mathbf{D}}^2 \hat{q}^k_j$ one obtains the scheme

$$\begin{aligned}(43)\qquad &\left[\lambda\mathbf{I}-(1+\lambda(j\alpha)^2)\tilde{\mathbf{D}}^{-2}\right]\hat{\xi}_j^k=(1+\lambda(j\alpha)^2)\hat{\delta}^k\\ &\hat{q}_j^k=\tilde{\mathbf{D}}^{-2}\hat{\xi}_j^k\\ &\hat{e}_j^k=\hat{\delta}^k+\hat{q}_j^k\ .\end{aligned}$$

Similar to the two-dimensional Poisson equation, we have to find the null-vector by solving the problem numerically. Again, this may be done in a preprocessing stage of the computation, with high accuracy. We find that due to the appearance of the parameter, λ, which may vary significantly for different computations, it is necessary to equilibrate the matrices prior to solving the problem by forward substitution. This is done in order to obtain maximum accuracy.

As for the treatment of the Poisson equation, we split the treatment of the solvability constraints into zero and non-zero Fourier modes.

Fourier mode $j \neq 0$:

Following the approach given by Eq.(28), the solvability constraints given in Eq.(40) for $\forall j \in [1,\ldots,N/2]$ are enforced as

$$\begin{aligned}&\sum_{i=0}^{M}B_{ij}^{+}\hat{\omega}_{ij}^{p}\ +\ \alpha_0\sum_{i=0}^{M}B_{ij}^{+}\hat{e}_{ij}^{0}\ +\ \alpha_1\sum_{i=0}^{M}B_{ij}^{+}\hat{e}_{ij}^{k}=0\\ (44)\qquad &\sum_{i=0}^{M}B_{ij}^{-}\hat{\omega}_{ij}^{p}\ +\ \alpha_0\sum_{i=0}^{M}B_{ij}^{-}\hat{e}_{ij}^{0}\ +\ \alpha_1\sum_{i=0}^{M}B_{ij}^{-}\hat{e}_{ij}^{k}=0\ .\end{aligned}$$

Note again that summation over the null-vectors may be performed as preprocessing.

Fourier mode $j = 0$:

As stated in Eq.(40), we have three consistent conditions from which we may choose two. We have chosen the conditions

$$\begin{aligned}&\sum_{\substack{i=0\\ i\ \text{even}}}^{M}\frac{\hat{\omega}_{i0}^{p}}{i^2-1}+\alpha_0\sum_{\substack{i=0\\ i\ \text{even}}}^{M}\frac{\hat{e}_{i0}^{0}}{i^2-1}+\\ (45)\qquad &\alpha_1\sum_{\substack{i=0\\ i\ \text{even}}}^{M}\frac{\hat{e}_{i0}^{1}}{i^2-1}=-\frac{C}{2L_x}\\ &\sum_{\substack{i=1\\ i\ \text{odd}}}^{M-1}i^2\hat{\omega}_{i0}^{p}+\alpha_0\sum_{\substack{i=1\\ i\ \text{odd}}}^{M-1}i^2\hat{e}_{i0}^{0}+\alpha_1\sum_{\substack{i=1\\ i\ \text{odd}}}^{M-1}i^2\hat{e}_{i0}^{1}=\end{aligned}$$

$$(46)\qquad \frac{1}{\nu L_x}\delta p-\frac{1}{2\nu}\frac{d}{dt}\left(U^+(t)+U^-(t)\right)\ ,$$

Equation (45) restricts the even modes by ensuring consistency between the circulation and the vorticity, and Eq.(46), obtained by adding the two Neumann conditions, restrains the odd modes of the vorticity. Again, we end up with a 2×2 system which has to be solved in order to obtain the remaining constants.

4.3 Initial vorticity distribution

The code is initialized by choosing a vorticity distribution at $t = 0$. This initial vorticity distribution must, naturally, sastisfy the no-slip boundary conditions (12). If the coefficients $\omega_{ij}(t=0)$ and $B_{ij}^{\pm}$ are considered as the components of M dimensional vectors for fixed $j \neq 0$, then the initial guess for $\widetilde{\omega}_{ij}(t=0)$ has to be projected onto a plane containing the vectors B_{ij}^{+} and B_{ij}^{-}. Since B_{ij}^{+} and B_{ij}^{-} are generally not mutually orthogonal, the two vectors

$$(47)\qquad b_{ij}^{e}=\frac{B_{ij}^{+}+B_{ij}^{-}}{2}\qquad\text{and}\qquad b_{ij}^{o}=\frac{B_{ij}^{+}-B_{ij}^{-}}{2}$$

are introduced. These two vectors are orthogonal to each other [9].

The projection of the initial guess for $\widetilde{\omega}_{ij}(t=0)$ onto the true no-slip $\omega_{ij}(t=0)$ is then performed by Gram-Schmidt orthogonalization

$$(48)\qquad \omega_{ij}=\widetilde{\omega}_{ij}-\frac{\widetilde{\omega}_{ij}\cdot b_{ij}^{e}}{\|b_{ij}^{e}\|^2}\,b_{ij}^{e}-\frac{\widetilde{\omega}_{ij}\cdot b_{ij}^{o}}{\|b_{ij}^{o}\|^2}\,b_{ij}^{o}\,.$$

In order for this projection scheme to give reasonable results, the initial guess $\widetilde{\omega}_{ij}$ should not be to far from satisfying the no-slip constraints (12). This can typically be achieved by choosing a zero-order distribution which gives rise to a flow parallel to the walls and adding an arbitrary, but not too large pertubation.

4.4 Asymptotic stability of the discrete scheme

As we aim at performing long time integration of the Navier-Stokes equations using the scheme described in the previous sections, we need to address the issue of temporal stability of the scheme.

The emphasis will be on asymptotic stability of the scheme ($t \to \infty$, Δt fixed) and not on the Lax-Richtmeyer stability ($\Delta t \to 0, t$ fixed). The concept of asymptotic stability is normally considered to be of main interest for practical purposes [16].

In order to perform the stability analysis, we linearize Eq.(1) around a linear velocity profile

$$\mathbf{u} = (y, 0) \ .$$

This recasts Eq.(1) into the linear form

$$\frac{\partial \omega}{\partial t} + y\frac{\partial \omega}{\partial x} = \nu \nabla^2 \omega \ ,$$

subject to the solvability constraints on the vorticity as derived in Sec. 3. Since the linear shear is unconditionally stable in the continuous case, this has to be true also for the fully discrete approximation.

We continue by expanding in a truncated Fourier-Chebyshev series to obtain two equations for the cosine and sine modes, respectively, for each Fourier mode $j \in [0, \ldots, N/2]$,

$$\frac{\partial \hat{\omega}_j^c}{\partial t} + (j\alpha)\mathbf{Y}\hat{\omega}_j^s = \nu \left[\mathbf{D}^2 - (j\alpha)^2\mathbf{I}\right] \hat{\omega}_j^c \tag{49}$$

$$\frac{\partial \hat{\omega}_j^s}{\partial t} - (j\alpha)\mathbf{Y}\hat{\omega}_j^c = \nu \left[\mathbf{D}^2 - (j\alpha)^2\mathbf{I}\right] \hat{\omega}_j^s \ . \tag{50}$$

Here $\hat{\omega}_j^c = (\hat{\omega}_{0j}^c, \ldots, \hat{\omega}_{Mj}^c)^T$ and likewise for $\hat{\omega}_j^s$, $\alpha = 2\pi/L_x$ is the aspect ratio of the channel, $\mathbf{D}^2$ is the 2nd order Chebyshev spectral differential operator and the convolution operator, $\mathbf{Y}$, is given as [16]

$$\mathbf{Y}_{ij} = \begin{cases} c_j \frac{1}{2} & j = i-1 \\ \frac{1}{2} & j = i+1 \\ 0 & \text{otherwise} \end{cases} \ ,$$

for $\forall i \in [0, \ldots, M]$, where $c_0 = 2$, $c_j = 1$ for $j > 0$ and $c_j = 0$ for $j < 0$.

For the semi-implicit predictor-corrector scheme given in Eq.(26), we obtain the following discrete approximation

$$\hat{\mathbf{L}}_j \hat{\omega}_j^* = \hat{\omega}_j^n - \frac{\Delta t}{12}(j\alpha)\hat{\mathbf{Y}}\left[23\hat{\omega}_j^n - 16\hat{\omega}_j^{n-1} + 5\hat{\omega}_j^{n-2}\right] \tag{51}$$

$$\hat{\mathbf{L}}_j \hat{\omega}_j^{n+1} = \hat{\omega}_j^n - \frac{\Delta t}{12}(j\alpha)\hat{\mathbf{Y}}\left[5\hat{\omega}_j^* + 8\hat{\omega}_j^n - \hat{\omega}_j^{n-1}\right] \ , \tag{52}$$

where we have introduced

$$\hat{\mathbf{Y}} = \mathbf{Y}\begin{bmatrix} 0 & \mathbf{I} \\ -\mathbf{I} & 0 \end{bmatrix} \text{ , and } \hat{\mathbf{L}}_j = \mathbf{L}_j \begin{bmatrix} \mathbf{I} & 0 \\ 0 & \mathbf{I} \end{bmatrix} \ ,$$

being the $2(M+1) \times 2(M+1)$ convolution operator and the discrete Helmholtz operator, $\mathbf{L}_j = \mathbf{I} - \nu\Delta t[\mathbf{D}^2 - (j\alpha)^2\mathbf{I}]$, respectively, for each Fourier mode. We assume that the solvability constraints for the vorticity, as given by Eq.(40) are introduced in $\mathbf{L}_j$ as tau conditions. We have also introduced the $2(M+1)$ vector $\hat{\omega}_j^n = [(\hat{\omega}_j^c, \ \hat{\omega}_j^s)^n]^T$.

The operations necessary to perform the predictor step, Eq.(51), may now conveniently be written in the form

$$\mathbf{A}\mathbf{x}^* = \mathbf{P}\mathbf{x}^n \ ,$$

where

$$\begin{aligned} \mathbf{x}^* &= (\hat{\omega}_0^*, \hat{\omega}_0^n, \hat{\omega}_0^{n-1}, \ldots, \hat{\omega}_{N/2}^*, \hat{\omega}_{N/2}^n, \hat{\omega}_{N/2}^{n-1})^T, \text{ and} \\ \mathbf{x}^n &= (\hat{\omega}_0^n, \hat{\omega}_0^{n-1}, \hat{\omega}_0^{n-2}, \ldots, \hat{\omega}_{N/2}^n, \hat{\omega}_{N/2}^{n-1}, \hat{\omega}_{N/2}^{n-2})^T \end{aligned}$$

are $3(M+1)(N+2)$ long vectors. Both $\mathbf{A}$ and $\mathbf{P}$ are $(N/2+1) \times (N/2+1)$ block diagonal matrices where each submatrix has the order $3(M+1) \times 3(M+1)$.

In a similar manner we may express the correction step, Eq.(52), on matrix form as

$$\mathbf{A}\mathbf{x}^{n+1} = \mathbf{C}\mathbf{x}^* \ ,$$

Combining these two expressions leads to

$$\mathbf{A}\mathbf{x}^{n+1} = \mathbf{C}\mathbf{x}^* = \mathbf{C}\mathbf{A}^{-1}\mathbf{P}\mathbf{x}^n \ .$$

Assuming $\mathbf{x}^n = \lambda^{-n}$ we obtain the generalized eigenvalue problem of $\mathcal{O}(3(M+1)(N+2))$

$$\mathbf{A}\mathbf{x}^n = \lambda\mathbf{C}\mathbf{A}^{-1}\mathbf{P}\mathbf{x}^n \ ,$$

by which we may show stability of the fully discrete scheme provided $|\lambda| \geq 1$. The eigenvalue problem may be solved using the QZ-algorithm. To limit the size of the actual computation, the eigenvalue problem for each Fourier mode may be treated separately.

In Figure 1 we show a typical spectrum obtained for $M = N = 24$, $\Delta t = 0.10$, $L_x = 2\pi$ and $\mathrm{Re} = 1/\nu = 100$. This clearly confirms that the total scheme is asymptotically stable and no numerical instabilities are introduced through the approximation of the continuous stable shear flow.

We observe that once the viscous boundary layer is resolved, which happens approximately for

$$M \geq \sqrt{\mathrm{Re}} \ ,$$

the stability of the explicit part of the time integration is well characterized by the Courant-Friedrichs-Levy criterion

$$CFL = \frac{|\mathbf{u}_{\max}|\Delta t}{\Delta x_{min}} \leq 1 \ .$$

A detailed discussion on the use of the CFL condition in spectral schemes is given in [17].

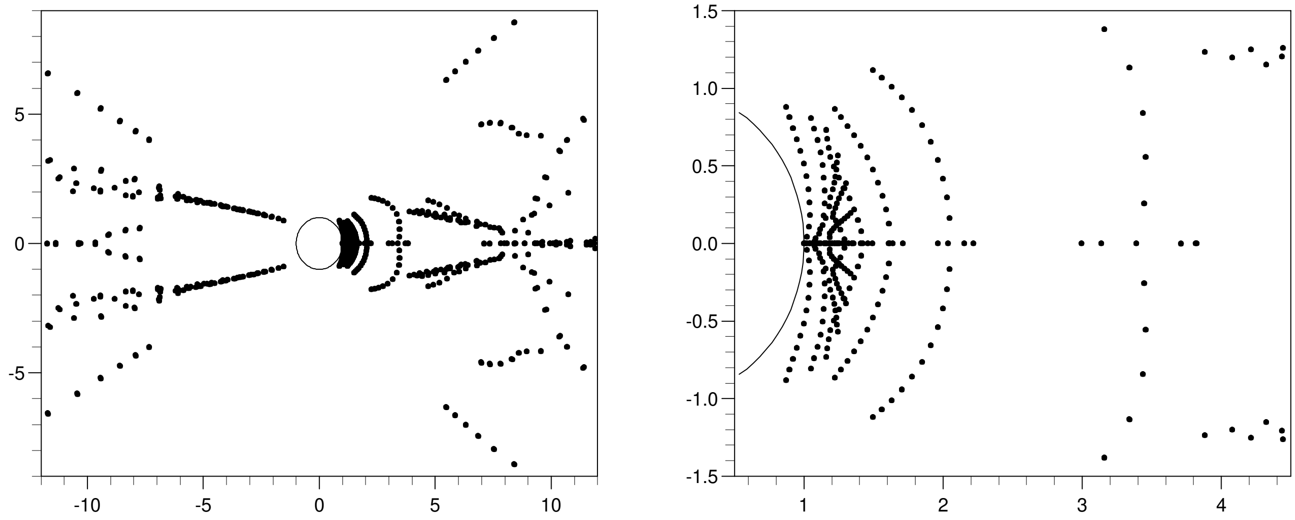

Figure 1: Characteristic eigenvalue spectrum for the fully discrete stability analysis for $M = N = 24$, $\mathrm{Re} = 1/\nu = 100$, $L_x = 2\pi$ and $\Delta t = 0.1$. *Left:* The spectrum around the unit circle. *Right:* Detail of the spectrum close to the unit circle.

For the case shown in Fig. 1, the CFL-criterion requires $\Delta t \leq 0.125$, which is supported by our results. We observe that as Δt increases, eigenvalues from the left half-plane moves towards the unit circle. In Fig. 1 we have used $\Delta t = 0.1$ and the scheme remains stable, but increasing the time step slightly implies that eigenvalues cross the unit circle and as a result the scheme becomes unstable.

5 Calculation of pressure field

The traditional approach of calculating the pressure is by taking the divergence of the momentum equation and enforcing the condition of incompressibility leading to the Poisson problem:

$$\nabla^2 p = \nabla \cdot (\rho \mathbf{u} \cdot \nabla \mathbf{u}) . \tag{53}$$

The boundary conditions are found by considering the momentum equation at the boundaries. Assuming fluid adhesion (no-slip) at the walls, the momentum equation

$$\mathbf{u}_t + \mathbf{u} \cdot \nabla \mathbf{u} = -\frac{1}{\rho} \nabla p + \nu \nabla^2 \mathbf{u}$$

gives

$$\nabla p|_{\partial \mathcal{D}} = -U'(t) + \nu \left. \nabla^2 \mathbf{u} \right|_{\partial \mathcal{D}}$$

where $U(t)$ is the wall velocity. This expression for the gradient of p gives rise to both Neumann and Dirichlet conditions on p, which leads to too many boundary conditions on the pressure. This problem can be overcome in a number of ways. However, there remains a serious accuracy issue. If the Navier-Stokes equations are solved in primitive variables, second-order derivatives of the velocity field must be calculated. If the $\omega - \psi$ form is used, then third-order derivatives must be taken since the computation of the velocity involves already a computation of $\nabla \psi$. Of course things are not necessarily drastically bad, since the stream function is calculated from the vorticity in spectral space by inverting the Laplace operator, and this procedure is smoothing. However, the problem of computing third derivatives can still be serious [6].

In our alternative approach, we avoid the issues related to overdeterminacy by rewriting the momentum equation in the form

$$\mathbf{u}_t + \omega \hat{\mathbf{z}} \times \mathbf{u} = -\nabla \left(\frac{p}{\rho} + \frac{1}{2} u^2 \right) - \nu \nabla \omega \times \hat{\mathbf{z}}$$

so that, introducing the dynamic pressure

$$P = p + \frac{1}{2} \rho u^2 ,$$

we obtain

$$\frac{1}{\rho} \nabla P = -\nabla \left(\psi_t + \nu \omega \right) \times \hat{\mathbf{z}} - \omega \nabla \psi .$$

Again, at first sight, calculating ψ_t involves high derivatives since

$$\nabla^2 \psi_t = -\omega_t = [\omega, \psi] - \nu \nabla^2 \omega .$$

However, this relation can be written as

$$\nabla^2 (\psi_t + \nu\omega) = [\omega, \psi]$$

This computes the lumped quantity $\psi_t + \nu\omega$ which, after all, is what appears on the right hand side of the pressure gradient equation. Thus, the need to consider anything but first derivatives in the pressure calculation is eliminated.

This leads to the following algorithm for the pressure computation:

- Given a vorticity field ω
- Find the values of the j-th Fourier mode of ω at walls, for $j \neq 0$:

$$\hat{\omega}_j(y = \pm 1) = \hat{\omega}_j^{\pm} = \sum_{i=0}^{M} (\pm 1)^i \hat{\omega}_{ij}, \quad j \neq 0$$

- Find ψ by solving the Poisson problems:

$$\nabla^2 \hat{\psi}_j = -\hat{\omega}_j \quad , \quad \hat{\psi}_j(y = \pm 1) = 0 \ , \ j \neq 0$$
$$\nabla^2 \hat{\psi}_0 = -\hat{\omega}_0 \quad , \quad \left.\frac{d\hat{\psi}_0}{dy}\right|_{y=\pm 1} = U^{\pm}(t)$$

- Compute the Jacobian $[\omega, \psi]$
- Compute the quantity $\psi_t + \nu\omega$:
  Solve
$$\nabla^2 (\psi_t + \nu\omega) = [\omega, \psi]$$
  subject to the boundary conditions
$$\left.\left(\hat{\psi}_{j,t} + \nu\hat{\omega}_j\right)\right|_{y=\pm 1} = \nu\hat{\omega}_j^{\pm} \quad , \quad j \neq 0$$
$$\frac{\partial}{\partial y}\left.\left(\hat{\psi}_{0,t} + \nu\hat{\omega}_0\right)\right|_{y=\pm 1} = -\frac{\delta p^{\pm}}{\rho L_x}$$
- Finally, compute $\omega \nabla \psi$
- Now consider the dynamic pressure $P = p + \frac{1}{2}\rho u^2$ which satisfies:
$$\frac{1}{\rho}\nabla P = -\nabla (\psi_t + \nu\omega) \times \hat{\mathbf{z}} - \omega \nabla \psi$$
  The right hand side is known, to an accuracy of the same order as the rest of the quantities involved in the code.

  We may compute the dynamic pressure in mode space by inverting either the x- or the y-component of the gradient. Each computation should produce the Fourier-Chebyshev expansion of P except for the corresponding 0-mode (i.e. inverting the x-component gives no information about the 0-Fourier mode, and, similarly, the y-component will yield no information about the 0-Chebyshev mode). Combining both computations we recover P. The two expansions thus constructed should agree on the non-zero modes. The difference of these two independent computations provides an upper estimate for the accuracy of the scheme.

6 Numerical tests

In previous papers [9, 18], the high accuracy of our method in calculations at moderate Reynolds numbers up to Re $\leq$ 3000 was demonstrated and close agreement with experimental results were shown.

Here, we will report results obtained by our code for higher Reynolds number flows in order to demonstrate the capabilities of the method.

6.1 Unstable Poiseuille flow

In the first example, we report results from direct simulations of a Poiseuille flow at Re $= 10,000$ and $\alpha = 2\pi/L_x = 1.0$. These parameters correspond exactly to the eigensolutions obtained for the Orr-Sommerfeld equation studied in Sec. 3.1. As we know the solution of the linearized problem with high accuracy, this procedure may be viewed as a thorough test of the full scheme and interdependencies of the spatial and temporal resolution.

In order to extract the unstable mode, we apply the algorithm by Buneman [19] which allows for calculating the frequency and growth rate of a monochromatic signal. It should be noted that this scheme is only second order accurate in time. As signal for the diagnostics we use the time-trace of the expansion coefficient of the second Chebyshev mode and the first Fourier mode, i.e. $k = 1$.

In all runs we used a time step, Δt, which is well under the limit dictated by the semi-implicit time advancing scheme. All runs have been continued until $T = 200$. The numbers are accurate to $\mathcal{O}(10^{-7})$.

In Table 3 we study the spatial convergence of the scheme. As found from the linear eigenvalue analysis in Sec. 3.1, we confirm that $M = 64$ and $N = 16$ is sufficient to resolve the dynamics of the unstable Poiseuille flow. We observe that as soon as the dynamics is resolved, we obtain the eigenvalues with very good accuracy.

We have also studied the temporal convergence of the full scheme. We find that the scheme is clearly first order

M	N	Δt	λ_i	λ_r
64	16	0.01250	0.2375063	0.0037167
64	32	0.01250	0.2375063	0.0037167
64	64	0.01250	0.2375063	0.0037167
64	128	0.01250	0.2375063	0.0037167
16	16	0.00625	0.2367990	0.0212072
32	16	0.00625	0.2396010	0.0042858
64	16	0.00625	0.2375164	0.0037283
128	16	0.00625	0.2375164	0.0037282

Table 3: Spatial convergence of frequency, λ_i, and growth rate, λ_r, for the unstable mode of a Poiseuille flow at Re=10,000, $k = 1, \alpha = 1.0$ and $U_0 = 1.0$. M and N are the number of Chebyshev and Fourier modes, respectively, and Δt designates the used time-step.

in time as expected from the backward Euler time step for the diffusive part of the equation.

6.2 Roll up between moving walls at high Reynolds number

In Figure 2 we show the evolution of the vorticity and pressure field during roll up of a thin shear layer in a periodic channel with counter moving walls at Reynolds number Re $= 40,000$. The value of Re is based on the channel half width and the total velocity difference between the upper and lower walls moving with $U^+ = -1$ and $U^- = 1$, respectively. Obviously, this example has mainly theoretical interest, since three-dimensional effects will begin to be important already at much lower Reynolds numbers. At $T = 0$, we have set up an unstable vorticity sheet perturbed in the x-direction by mode number 1. In this example, we have used 512 Fourier modes and 1024 Chebyshev modes, corresponding to 342×684 active modes after de-aliasing. The time step, Δt, is 10^{-3}.

We observe a very high degree of symmetry in the numerical solution despite many violent bursts of boundary layer vorticity. Symmetry of the flow is maintained up to $T \approx 35$. After this, the code can no longer adequately resolve the dynamics and breaks down shortly after $T = 37$. We have performed a similar simulation [20] with additional random noise of amplitude 10^{-8} added to all the spectral modes at $T = 0$. This slightly noisy run begins to lose symmetry at $T \approx 20$, indicating that round-off errors in the present calculation are less than 10^{-8}.

The accuracy checks described in Sec. 2.1 for the energy and enstrophy evolution give $5 \cdot 10^{-4}$ accuracy for dE/dt and $5 \cdot 10^{-2}$ for $d\Omega/dt$ at $T = 24$. At $T = 30$, these numbers are $2 \cdot 10^{-2}$ and 10^{-1}, respectively, indicating the loss a adequate resolution near the end of the simulation. We would like to emphasize that these accuracy tests, and especially the enstrophy evolution test, are very valuable diagnostic tools, since they provide consistency checks for the complex dynamics involved in vorticity production during boundary layer eruptions.

The computation of the pressure gives global errors, as defined in the last part of Sec. 5, of $\mathcal{O}(10^{-7})$ up to $T \approx 5$, when thin boundary layers near the walls are formed. The global error then grows to $\mathcal{O}(10^{-5})$ which is kept throughout the symmetric evolution, demonstrating the high accuracy of the pressure algorithm.

7 Concluding remarks

In this paper, we have developed a spectral tau method for the solution of the incompressible Navier-Stokes equations in a planar geometry. The emphasis has been on the periodic channel with no-slip walls, but we have previously employed similar algorithms in annular geometries [3, 7, 18], just as we are presently adapting the scheme to a disk geometry.

The emphasis in this work has been on the accurate solution of the incompressible Navier-Stokes equations for flows with strong boundary layer interactions. Such flows require high spatial resolution, which, in turn, impose severe requirements on the development of accurate and efficient algorithms. We have implemented several diagnostic accuracy tests in the code, and in the present paper, we have reported results demonstrating that high accuracy can be obtained even for flows with violent boundary layer activity.

We have previously demonstrated close agreement [3, 7, 18] between our numerical results and experiments performed at moderate Reynolds numbers, $\mathcal{O}(1000)$. In this paper, we have furthermore demonstrated the ability of our scheme to perform accurate and direct simulations of turbulent boundary layer eruptions in planar flows at Reynolds numbers which are even an order of magnitude higher.

Acknowledgments

Part of this work was performed while one of the authors (EAC) visited Risø National Laboratory, Denmark, and another part was performed while the two other authors (JPL and JSH) visited the University of New Mexico, Albuquerque, USA. These visits have played an important role in the development of the spectral methods employed in this paper and they are gratefully acknowledged. One of the authors (JSH) was partially supported by the Danish

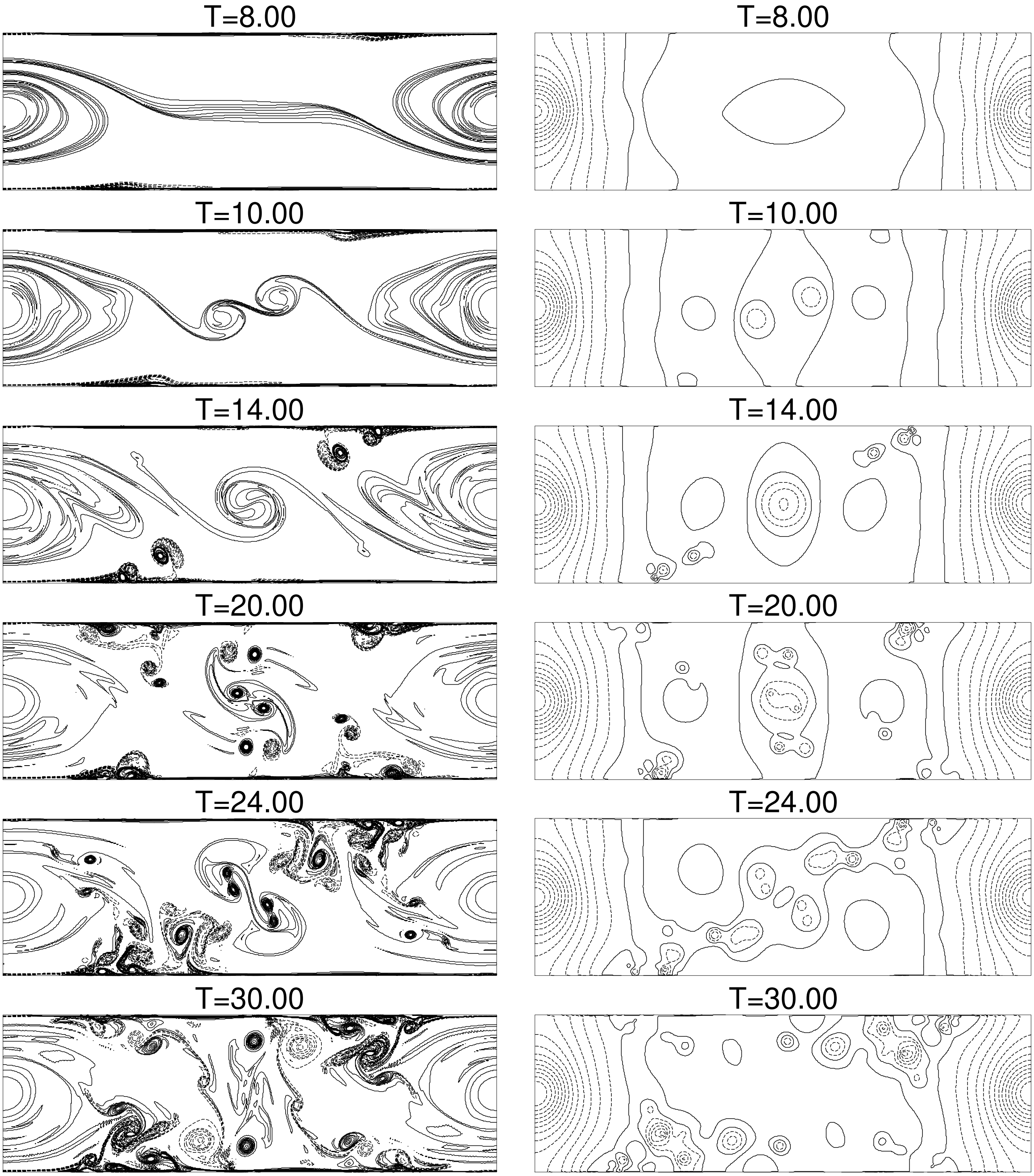

Figure 2: The roll up of a thin shear layer in a periodic channel with counter moving walls at Re = 40,000. The contour plots show vorticity (left) and pressure (right) with full and dashed lines indicating positive and negative levels, respectively.

Computing Center for Research and Education (UNI•C) and by the Danish Science Academy. The research was supported in part by DOE Grant DE-FG03-92ER25128, and the use of computer resources was supported by the Danish Research Councils.

References

[1] G.J.F. Van Heijst and J.B. Flor, *Laboratory experiments on dipole structures in a stratified fluid*, in Mesoscale/Synoptic Coherent Structures in Geophysical Turbulence, eds. J.C.J. Nihoul and B.M. Jamart, Elsevier, 1989, pp. 591–608.

[2] S.I. Voropayev and Ya.D. Afanasyev, *Symmetric interaction of developing horizontal jet in a stratified fluid with a cylinder*, Phys. Fluids, 6 (1994), pp. 2032–2037.

[3] E.A. Coutsias, J.P. Lynov, A.H. Nielsen, M. Nielsen, J. Juul Rasmussen and B. Stenum, *Vortex dipoles colliding with curved walls*, in Future Directions of Nonlinear Dynamics in Physical and Biological Systems, eds. P.L. Christiansen et al., Plenum Press, 1993, pp. 51–54.

[4] S.J. Barker and S.C. Crow, *The motion of two-dimensional vortex pairs in a ground effect*, J. Fluid Mech., 82 (1977), pp. 659–671.

[5] J. Homa, M. Lucas and D. Rockwell, *Interaction of impulsively generated vortex pairs with bodies*, J. Fluid Mech., 197 (1988), pp. 571–594.

[6] W.S. Don and A. Solomonoff, *Accuracy and speed in computing the Chebyshev collocation derivative*, submitted to SIAM J. Sci. Comp.

[7] E.A. Coutsias, K. Bergeron, J.P. Lynov, and A.H. Nielsen, *Self organization in 2D circular shear layers.* AIAA paper 94-2407 (1994), pp. 1–11.

[8] E.A. Coutsias, T. Hagstrom, and D. Torres, *An efficient spectral method for ordinary differential equations with rational function coefficients*, Math. Comp. - to appear (1995).

[9] E.A. Coutsias and J.P. Lynov, *Fundamental interactions of vortical structures with boundary layers in two-dimensional flows*, Physica D, 51 (1991), pp. 482–497.

[10] S.C.R. Dennis and L. Quartapelle, *Direct solution of the vorticity-stream function ordinary differential equations by a Chebyshev approximation*, J. Comput. Phys., 52 (1983), pp. 448–463.

[11] C.R. Anderson, *Vorticity boundary conditions and boundary vorticity generation for two-dimensional viscous incompressible flows*, J. Comput. Phys., 80 (1989), pp. 72–97.

[12] H.D. Nguyen, S. Paik and J.N. Chung, *Application of vorticity integral conditioning to Chebyshev pseudospectral formulation for the Navier-Stokes equations*, J. Comput. Phys., 106 (1993), pp. 115–124.

[13] E.A. Coutsias and J.P. Lynov, *Accurate computation of vorticity no-slip constraints*, in preparation.

[14] S.A. Orszag, *Accurate solution of the Orr-Sommerfeld equation*, J. Fluid Mech., 50 (1971), pp. 689–703.

[15] G.H. Golub and C.F. Van Loan, *Matrix computations*, 2nd Ed., Johns Hopkins University Press, Baltimore, 1993.

[16] D. Gottlieb and S.A. Orszag, *Numerical analysis of spectral methods: Theory and applications*, SIAM-CBMS 26, Philadelphia, 1977.

[17] D. Gottlieb and E. Tadmor, *The CFL condition for spectral approximations to hyperbolic initial-boundary value problems*, Math. Comp., 56 (1991), pp. 565–588.

[18] J.P. Lynov, E.A. Coutsias and A.H. Nielsen, *A spectral algorithm in the vorticity-stream function formulation for two-dimensional flows with no-slip walls*, in Computational Fluid Dynamics '92, eds. Ch. Hirsch et al., Elsevier, 1992, pp. 413–420.

[19] O. Buneman, *Diagnosing oscillatory growth or decay*, J. Comput. Phys., 29 (1978), pp. 295–296.

[20] J.P. Lynov, E.A. Coutsias and J.S. Hesthaven, *New spectral algorithms for accurate simulations of bounded flows*, in proc. of "Advanced concepts and techniques in thermal modelling. Eurotherm 36.", Poitiers, France, 1994, pp. N16–N21.